water

MDPI

Article

Hydrogeophysical and Hydrochemical Assessment of the Northeastern Coastal Aquifer of Egypt for Desalination Suitability

Mohamed Abdelfattah [1,*], Heba Abdel-Aziz Abu-Bakr [2], Farag M. Mewafy [3], Taher Mohammed Hassan [2], Mohamed H. Geriesh [4], Mohamed Saber [5] and Ahmed Gaber [1]

1 Geology Department, Faculty of Science, Port Said University, Port Said 42522, Egypt
2 Research Institute for Groundwater, National Water Research Centre, Cairo 13621, Egypt
3 Boone Pickens School of Geology, Oklahoma State University, Stillwater, OK 74078, USA
4 Geology Department, Faculty of Science, Suez Canal University, Ismailia 41522, Egypt
5 Water Resources Research Center, Disaster Prevention Research Institute, Kyoto University, Kyoto 611-0011, Japan
* Correspondence: mohamed_abdelfatah@sci.psu.edu.eg; Tel.: +20-10-1240-9010

Abstract: Recently the limited freshwater resources have become one of the most significant challenges facing Egypt. Thus, new resources of drinkable water are required to meet the growing population demands and the national projects, to support the country's economy. Saline groundwater desalination is an option that can support limited freshwater resources. This research represents a detailed analysis of hydrogeological and hydrochemical characteristics of a coastal aquifer in the West Port Said area, northeastern Egypt, to assess the desalination suitability of the aquifer, especially when the nearby seawater is contaminated. The hydrogeological characterization included various integrated approaches: geophysical survey, field investigations, wells drilling, well logging, pumping tests, and water sampling. The results show that: (1) The subsurface lithology consists of sandstone and clay, and three water bearing layers: A, B and C. (2) The average porosity values are 22%, 27.5%, and 25% for layers A, B, and C, respectively. The hydraulic conductivity values fall in the ranges of 5.8–12.7 m/day for layer A, 7.6–11.7 m/day for layer B, and 11.1–19.5 m/day for layer C, while the highest transmissivity values are in ranges of 5.8×10^2–12.7×10^2 m^2/day for layer A, 7.6×10^2–11.7×10^2 m^2/day for layer B and 11.1×10^2–19.5×10^2 m^2/day for layer C. (3) The average storage values are 2.1×10^{-3}, 1.8×10^{-3} and 5.3×10^{-3} in layers A, B and C, respectively. (4) Layers A and B showed Na-Cl-type, similar to seawater, but free from oil pollution. These results show layer B's higher productivity and better quality. Despite the salinity, desalination technology can improve.

Keywords: desalination; groundwater characteristics; geophysical technique; water quality; coastal area; Egypt

Citation: Abdelfattah, M.; Abu-Bakr, H.A.-A.; Mewafy, F.M.; Hassan, T.M.; Geriesh, M.H.; Saber, M.; Gaber, A. Hydrogeophysical and Hydrochemical Assessment of the Northeastern Coastal Aquifer of Egypt for Desalination Suitability. *Water* **2023**, *15*, 423. https://doi.org/10.3390/w15030423

Academic Editor: José Luis Sánchez-Lizaso

Received: 6 December 2022
Revised: 5 January 2023
Accepted: 17 January 2023
Published: 20 January 2023

1. Introduction

The world's fresh water crisis is expected to worsen in the near future [1]. Freshwater availability in arid and semi-arid regions is constantly threatened by growing population rates and related demands [2]. Egypt is one of the regions that faces a major shortage of freshwater resources. Some of the driving factors of this shortage are the very low precipitation rates and the continuous increase in water demand due to Egypt's continuously expanding population [3]. Thus, the country's main focus is to find alternative freshwater sources.

Desalination is one of several proposed technical approaches to solve the freshwater crisis [4]. According to previous studies, around 60% of the source water for desalination originates from saltwater, 20% from saline groundwater, and the remaining 20% comes

from surface water and saline wastewater [5]. Reverse osmosis (RO), which dominates the desalination industry globally, has a capacity of around 97 million m^3 now, and by 2025, it is predicted that market revenue will reach USD 27 billion [6,7].

West Port Said is a coastal area in northeastern Egypt that has recently expanded to include several urban, touristic, and industrial development areas that require water supplies. The only method to guarantee a constant water supply in such regions is water desalination, which often relies on seawater [8]. However, this area lies in the vicinity of the already oil-polluted transit zone of the Suez Canal's north entrance. This makes seawater desalination a problematic approach. An oil spill was previously observed within the area [9].

The research area is a portion of the Nile Delta aquifer, one of the world's largest groundwater reservoirs [10], with a total capacity of 500 Bm^3 [11]. Thus, the Nile Delta has been the focus of various studies in recent decades, including in geology [12–14], land subsidence and sea-level rise (SLR) [15,16], geochemistry [17,18], and hydrogeology [19]. The Nile Delta aquifer (NDA) extract groundwater is highly utilized [20], and simultaneously, the aquifer recharge is threatened by salt water intrusion (SWI). This phenomenon is common in coastal aquifers all over the world and is mostly caused by excessive groundwater pumping [21]. Other causes of salt-water intrusions include global sea level rise [22], seasonal changes in groundwater table levels [22], and groundwater tides [23]. Preventing hazards to water in various situations is crucial [24].

In contrast to seawater, saline groundwater (SGW) desalination is expected to have various advantages, such as: (1) Feedwater pretreatment is not required due to the natural filtration of groundwater through porous sediment, which means a reduction in the treatment plant area [25,26]. (2) The groundwater temperature variation is low (24 °C) and falls within the desalination temperature range [27]. (3) The fresh saline interference (FSI) moves toward the sea when salty groundwater is pumped underneath it, which may eliminate seawater intrusion into coastal aquifers [28,29]. (4) SGW is expected to result in less fouling on RO membranes than coastal seawater due to lower levels of various RO desalination-related characteristics, such as total organic carbon (TOC), dissolved oxygen (DO), turbidity, and silt [27,30–32]. (5) SGW desalination plants have lower operating costs over longer periods of operation, despite the fact that the initial cost of an SGW intake system is higher than that of a seawater intake system [26,33]. Various locations throughout the world have used SGW desalination in coastal aquifers over the past decade, including Malta [25], Spain [34], Saudi Arabia [35], Kuwait [36], Oman, and the Turks and Caicos Islands [37].

The goal of this research is to assess the hydrogeological and hydrogeochemical characteristics of the coastal aquifer in West Port Said and to ascertain its suitability for desalination. The study's findings will be beneficial to the community and taken into consideration, especially because of the presence of a desalination plant in the study region. It is necessary to thoroughly investigate the detailed subsurface study area. Therefore, geophysical exploration techniques, groundwater chemical analysis, well logging, pumping tests, and sediment analysis were performed. This approach could help in improving the coastal groundwater quality for long-term sustainable water resource management.

2. The Study Area

The study area is situated in West Port Said City in the northeastern Nile Delta, Egypt (Figure 1a). It extends from 32°4′57″ to 32°5′18″ east and from 31°21′ to 31°21′12″ north. It covers an area of approximately 25 km^2 and is characterized by a flat topography that does not exceed more than five meters above sea level. The coastal sand dunes (Figure 1c), which are concentrated on the north side of the study region (along the coast), and the sabkha, which is concentrated in the southern section, are the dominant geomorphic features of the study area.

Along the Mediterranean Sea coast, the study area is characterized by daily average temperatures that range from 17 to 20 °C [38]. In the morning and evening, the annual

mean relative humidity values are 60% and 80%, respectively [39]. The highest average yearly rainfall amount in the previous 12 years was 64 mm in 2015, and the study area's maximum monthly rainfall average was 50 mm [40]. As a result, the amount of rain in the examined area does not aid in the recharging of the aquifer.

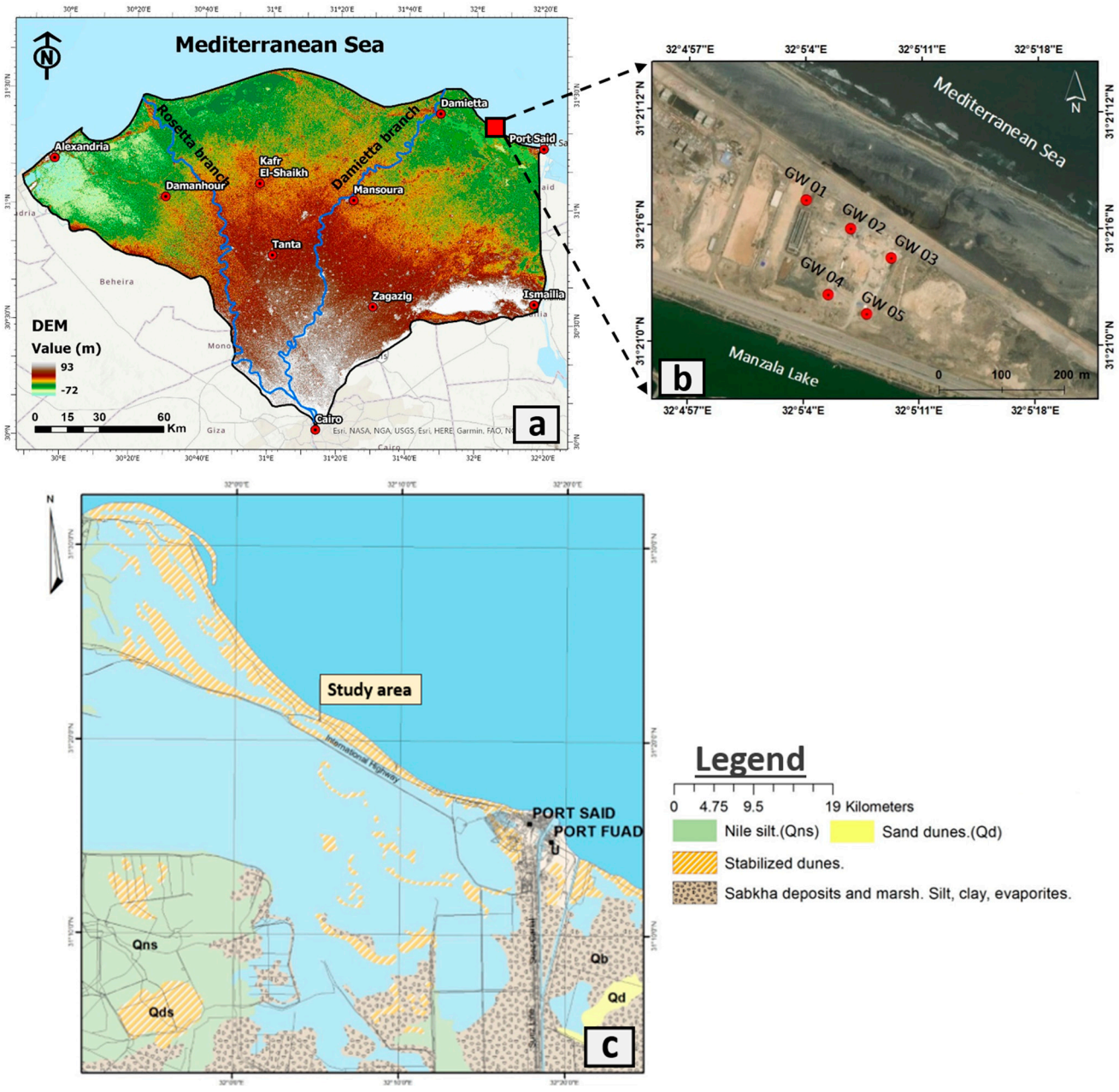

Figure 1. (**a**) The topography of Nile Delta, Egypt. (**b**) The study area with five test wells. (**c**) Geomorphologic units along the study area [41].

2.1. Geological Setting

According to previous studies and field investigations, both Quaternary and Tertiary deposits are the two basic geological components in the study area. The Holocene sediments are extensively distributed, with a maximum thickness of 77 m [42]. Furthermore, the thickness of the Quaternary deposits increases northward, reaching 250 m in the south and 1000 m in the north [43]. Quaternary sediments are definitely present in the studied region [42]. These deposits comprise gravel and sand with some clay lenses from the Holocene and Pleistocene Bilqas, Mit Ghamr, and Wastany formations [44].

2.2. Hydrogeological Setting

The North Delta aquifer (NDA) is a substantial groundwater aquifer and semi-confined groundwater system [14]. This geological layer contains groundwater at shallow depths of 1.0 to 1.5 m below the surface. Due to the limited permeability of the clay and silt strata, the specific yield of the Holocene aquifer is quite low [45]. The major aquifer of the entire NDA is the Pleistocene aquifer, which encompasses the entire Nile Delta and is quite productive. Its thickness varies from 200 m in the south to 1000 m in the north [20].

In the study region, five tested production wells (Figure 1b) are drilled to provide more effective hydrogeological studies of the coastal aquifer. The shallow wells (GW01 and GW05) were drilled to reach total depths of 62 m and 70 m, respectively. These wells were designed with screen depths of 30–60 m and 30–70 m, respectively. Meanwhile, the deep wells (GW02, GW03, and GW04) were drilled to reach total depths of 400 m, 220 m and 500 m, respectively. These wells were designed with screen depths of 120–300 m, 100–200 m, and 370–500 m, respectively. According to measurements of the static water levels in the five wells within the research area, the shallow wells (GW01 and GW05) ranged from 1.4 to 0.9 m and from 1.4 to 1.1 m, respectively. Meanwhile, the deep wells (GW02, GW03, and GW04) had groundwater levels that ranged from 0.6 to 1 m, from 0.8 to 1.1 m, and from 0.5 to 0.8, respectively.

The inflow budget in the study area has one component, inflow across boundaries, while the outflow budget has two components, outflow across boundaries and groundwater withdrawal from wells [44]. Figure 2 illustrates the groundwater flow in and around the study area, showing that it gradually moves from the Mediterranean Sea to Manzala Lake in the south [44]. Therefore, the aquifer is dominated by the Na-Cl type and has a high TDS, with increased concentrations of major ions.

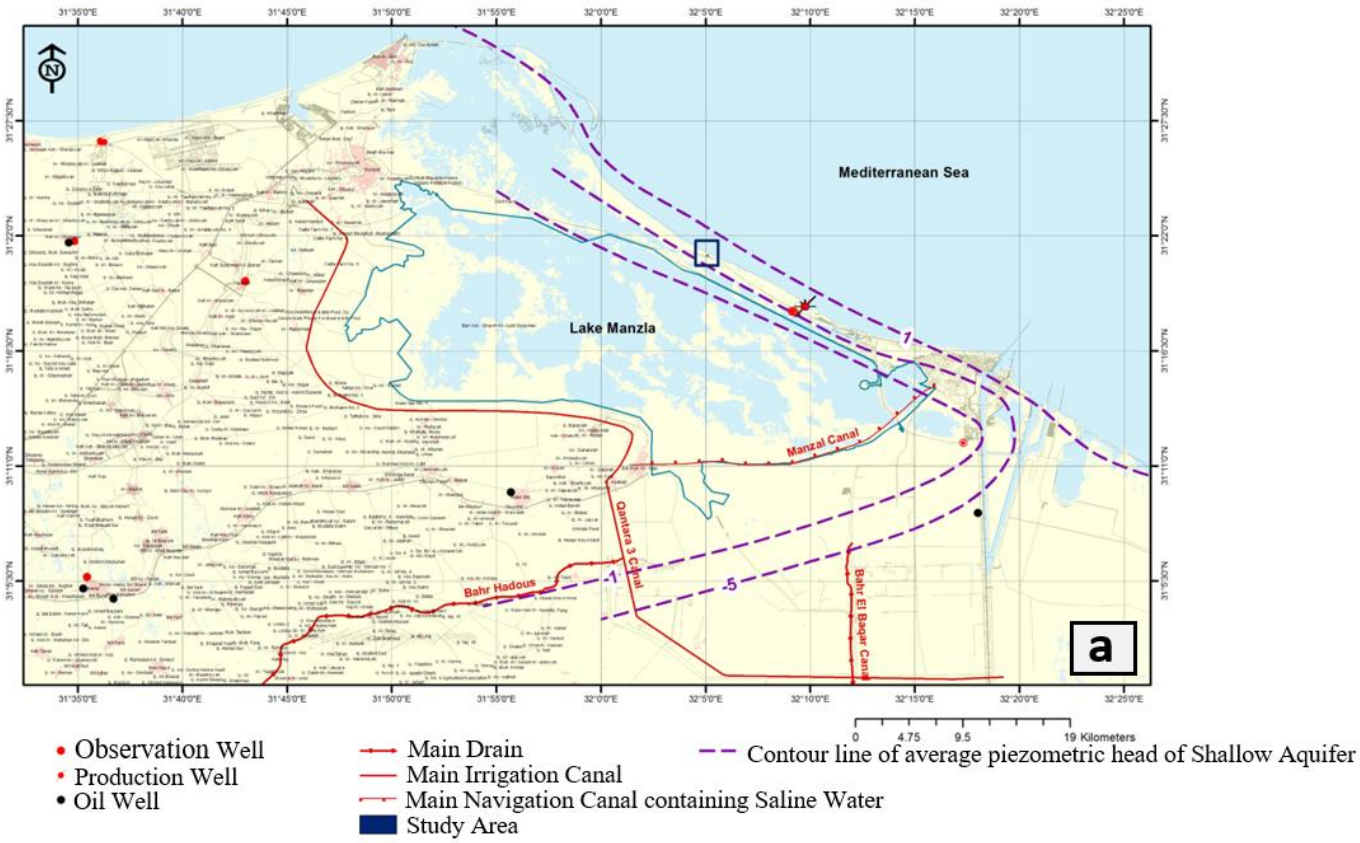

Figure 2. *Cont.*

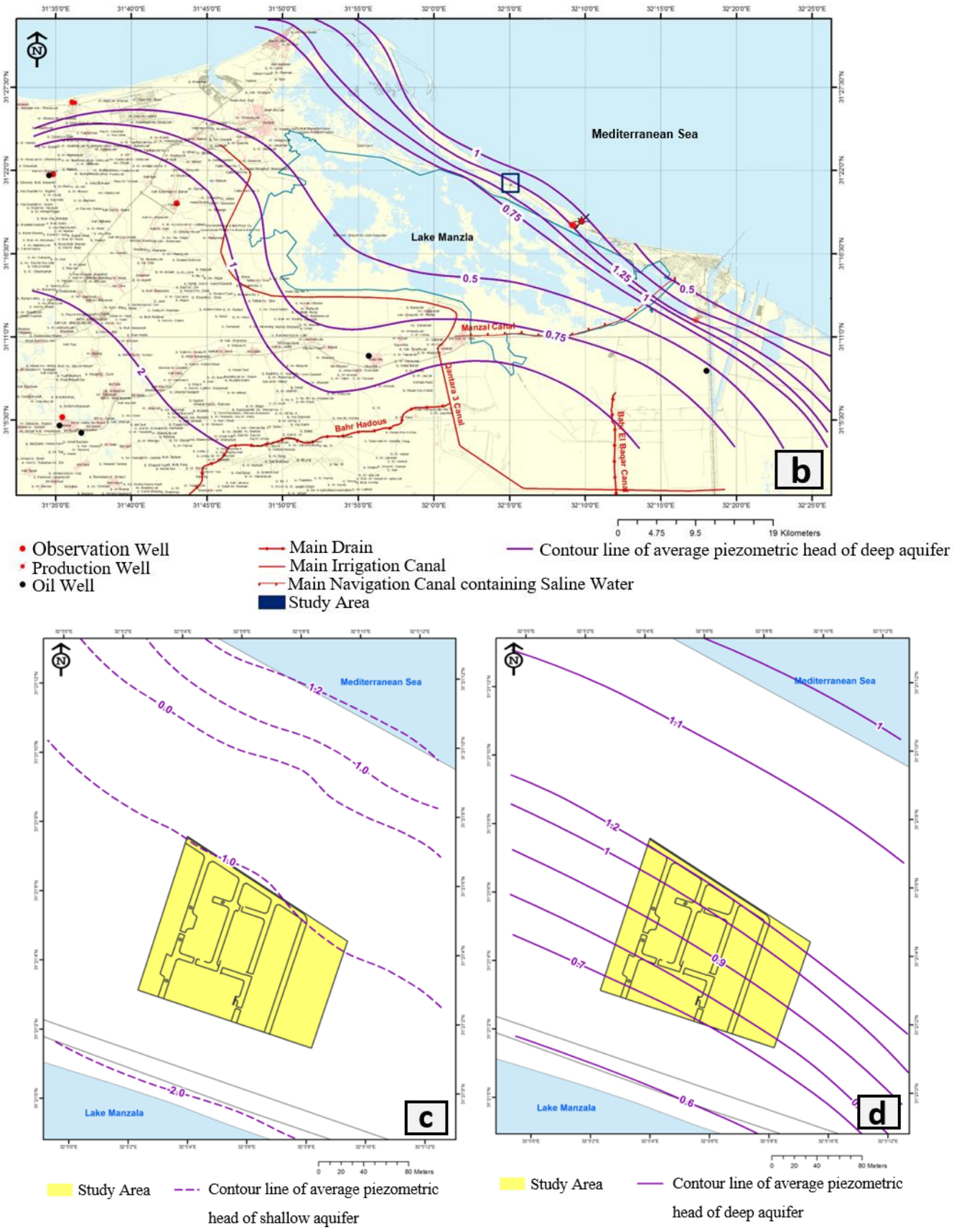

Figure 2. Regional and local groundwater levels for layer A (**a**,**c**) and layer B (**b**,**d**).

3. Materials and Methods

Figure 3 illustrates the integration of the techniques utilized to achieve the study's goal. First, we determined the topography and climatic factors of the research location. Following the start of the field work, the most appropriate geophysical methods were used to explore the groundwater, identify the subsurface layers, and determine the depth of the water level. In addition to obtaining the hydrogeological information of drilling wells, well pumping tests and sediment analyses were also used to ascertain the properties of the various layers of the reservoir. Finally, by analyzing of major ions and heavy metals in the groundwater samples, we could evaluate of the reservoir's quality.

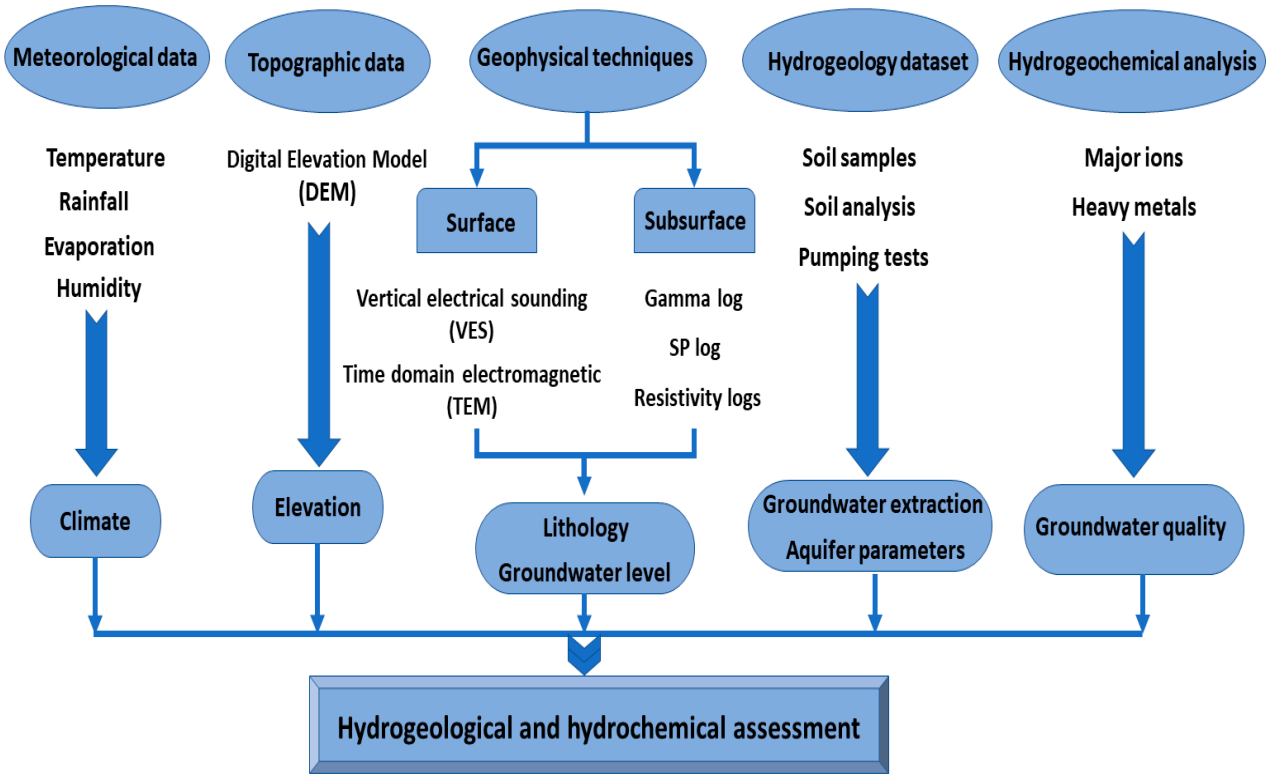

Figure 3. Flow chart of the used methodological steps.

3.1. Geophysical Techniques

3.1.1. Resistivity and Time Domain Electromagnetic Methods

The most popular approaches in hydrological applications are vertical electrical sounding (VES) and transient electromagnetic (TEM) techniques.

In this investigation, 2 VES soundings were performed utilizing a one-dimensional Schlumberger array with a maximum current electrode spacing (AB) of 600 m to penetrate reasonably deep, particularly near the exploration wells in the southern portion of the study region. The field measurements started at two meters between the current's poles and increased up to 600 m to learn about the underlying sequences and recognize the various aquifer layers. The SAS-300 system was employed, which records changes in ground resistance values quite accurately. The AIE-2 TEDM system conducted a total of eight transient electromagnetic (TEM) soundings. These eight soundings were performed in the research area's northern region, where it was practical to conduct them. Single loops of 50 × 50 m and 100 × 100 m were carried out at TEM sites 2, 3, and 4, whereas the single loops of 150 × 150 m were carried out at TEM sites 1 and 5. Finally, the 1X1D program was used to integrate VES and TEM results with the underlying soil model created from the very nearby drilled well in order to determine the true resistivity values for the various geoelectric layers and generate electromagnetic and geoelectric cross sections (Figure 4).

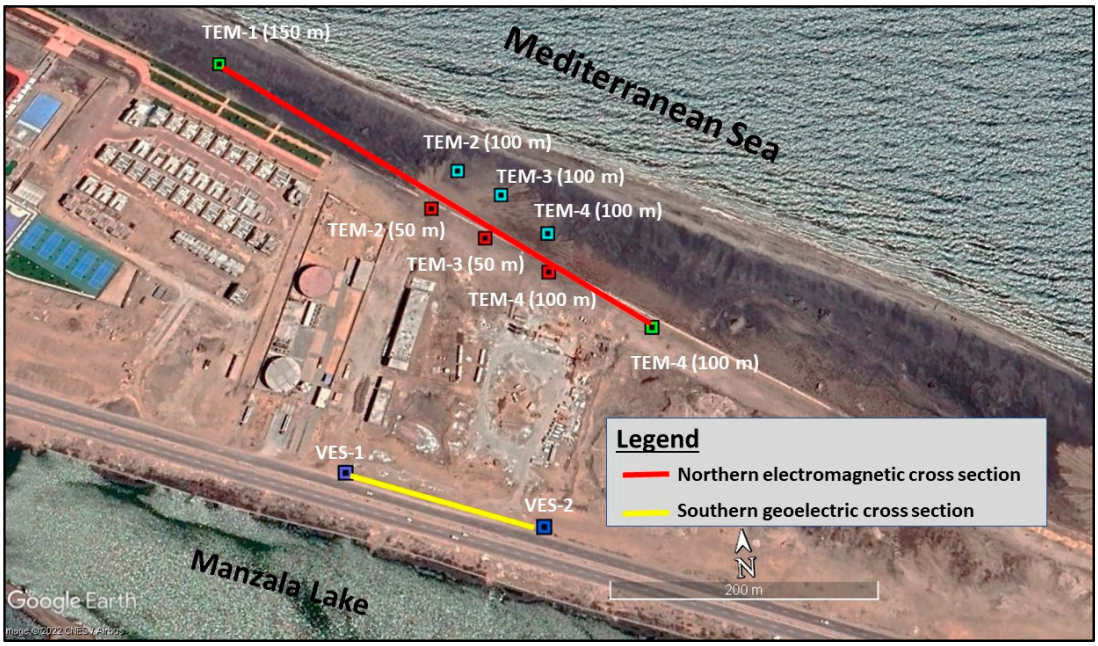

Figure 4. Map represents the locations of VES and TEM measurements and their cross-sections within the study area.

3.1.2. Well Logging

Numerous geophysical methods are employed for subsurface hydrogeological applications; however, geophysical well logging is a useful tool for assessing the underlying lithologic and hydrologic conditions [46–49]. This type of survey provides in-situ information regarding the physical characteristics of the underlying strata (such as resistivity, radioactivity, and permeability) and groundwater quality [50]. Three geophysical well loggings were carried out within the study area for three wells (GW02, GW04 and GW05) at depths of 400 m, 500 m, and 70 m, respectively (Figure 5a). In each well, a gamma ray log, self-potential (SP) log, and short normal resistivity and long normal resistivity logs were performed.

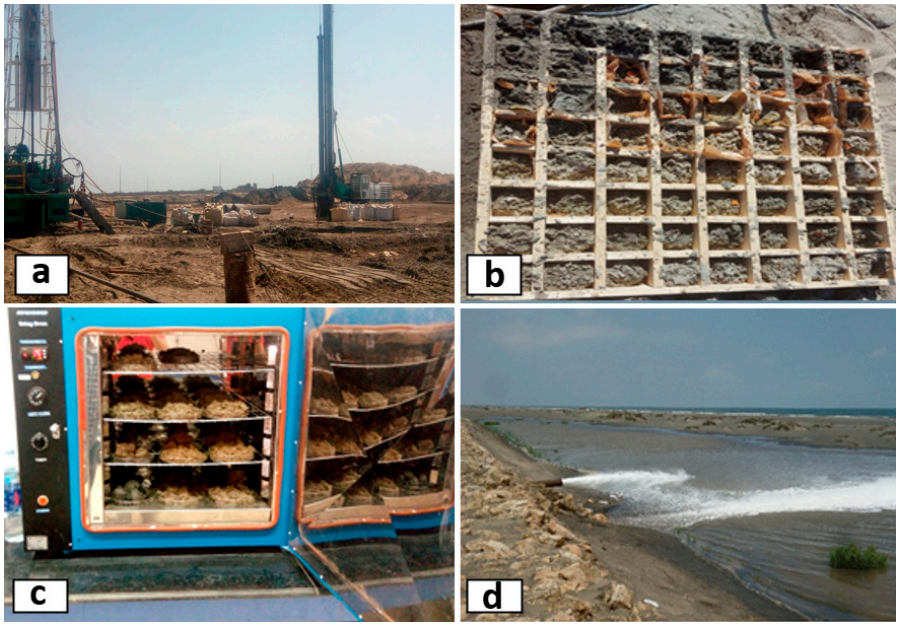

Figure 5. (**a**) Drilling of wells in the study area, (**b**) sediment samples during drilling of wells, (**c**) drying the sediment sample in the oven, and (**d**) during the pumping test of well.

3.2. Hydrogeological Characterization

3.2.1. Sediment Analysis

Sediment samples were collected every meter in each well during drilling. To determine the porosity of sandstone samples from three aquifers (Figure 5b), the following sandstone samples were selected from each well:

- GW01: At depths of 5, 10, 35, 50, and 60 m;
- GW05: At depths of 5, 40, 45, 50, 55, and 60 m;
- GW 02: At depths of 120, 140, 180, 250, 270, 300, and 320 m;
- GW03: At depths of 110, 150, 200, and 210 m;
- GW04: At depths of 360, 370, 390, and 380 m.

The sediment samples were dried in an oven (Figure 5c) at 105 °C for 24 h using the gravitational (weighting) method, and the saturation moisture content was then computed [51]. Subsequently, the total porosity was estimated as the ratio of the total volume of saturation water to the entire soil volume. Finally, the average porosity values of the three aquifers were determined based on the boundaries of each aquifer.

3.2.2. Pumping Test

Pumping test experiments were performed at five wells in the research region as part of this investigation. After the development and construction were finished, step and continuous pumping testing were conducted at each well (Figure 5d). The two most important measurements made during the pumping test are the pumping rate (or discharge) and changes in the water levels in both the observation well and the pumping well.

The hydraulic parameters of five wells were estimated using the Hantush 1960 and Thesis 1935 pumping test analysis methods, as follows, depending on the type of aquifer used for the withdrawal. These parameters included the vertical hydraulic conductivity, the storage coefficient of the aquitard, and the transmissivity and storativity of the pumped aquifer:

- GW01: Based on Theis's pumping analysis with Jacob's correction for unconfined aquifers;
- GW05: Based on Theis's pumping tests with Jacob's correction for unconfined aquifers;
- GW02: In accordance with Theis's pumping analysis for confined aquifers;
- GW03: Based on Hantush's analysis of pumping tests for leaky confined aquifers;
- GW04: In accordance with Theis's analysis of pumping tests for confined aquifers.

3.2.3. Groundwater Sampling and Analysis

Six groundwater samples were gathered from shallow wells (GW01 and GW05) and deep wells (GW2 and GW03) to represent the groundwater quality of unconfined (layer A) and leaky aquifers (layer B), respectively, as follows:

- The W1 water sample was collected from well GW01;
- The W2 and W3 water samples were collected from well GW05;
- The W4 and W5 water samples were collected from well GW02;
- The W6 water sample was collected from well GW03.

These samples were gathered in 1000 mL pre-washed, clean polyethylene plastic bottles, and they were kept refrigerated at 4 °C. The chemical analysis was conducted in accordance with the recommended standards by [52]. The hydrochemical analyses of the groundwater samples are performed at the Groundwater Research Institute of the Ministry of Water Resources and Irrigation since it is one of the authorized locations, which confirms to the excellent accuracy of the study's findings. The chemical analyses included the major cations (Na^+, K^+, Ca^{2+}, Mg^{2+}), the anions (HCO_3^-, CO_3^-, SO_4^{2-}, Cl^-,and NO_3^-), fluoride (F^-), and heavy metals (Al, Sb, As, Ba, Cd, Cr, Co, Cu, Fe, Pb, Mn, Ni, and Se) by using inductively coupled plasma (ICP-OES). the groundwater samples were examined in-situ, particularly during the pumping tests of the wells, for their temperature, pH, total dissolved solids (TDS), and electrical conductivity (EC). Durov plots (1984) were used to represent the data analyses [53].

4. Results

4.1. Subsurface Lithology

A total of five wells were drilled in the study area, as previously described. In three of these wells (GW02, GW04, and GW05), the well logging technique was utilized to identify the lithology of the sub-surface strata and their boundaries, thereby determining the water-bearing layers. To accomplish this goal, geophysical well logs (gamma ray, spontaneous electrical potential (SP), and resistivity logs) were used.

Integrating the findings from the northern and southern geophysical cross sections (Figures 6 and 7), well logs of the wells (Figures 8–10), additional drilling data from wells in the study region (GW01 and GW03), and data from supplemental wells in the neighborhood, it is obvious that the lithology is composed of gravel and sand with clay lenses that date to the Holocene and Pleistocene (Bilqas, Mit Ghamr, and Wastany formations). The water bearing layers were identified and divided into three layers:

- The first layer (A) ranges from 0 to 90 m in depth and is composed of medium to fine sandstone with intercalation of clay layers;
- The second layer (B) ranges from 110 to 310 m depth and is composed of coarse to medium sandstone;
- The third layer (C) ranges from 330 to 500 m in depth and composed of coarse to medium sandstone.

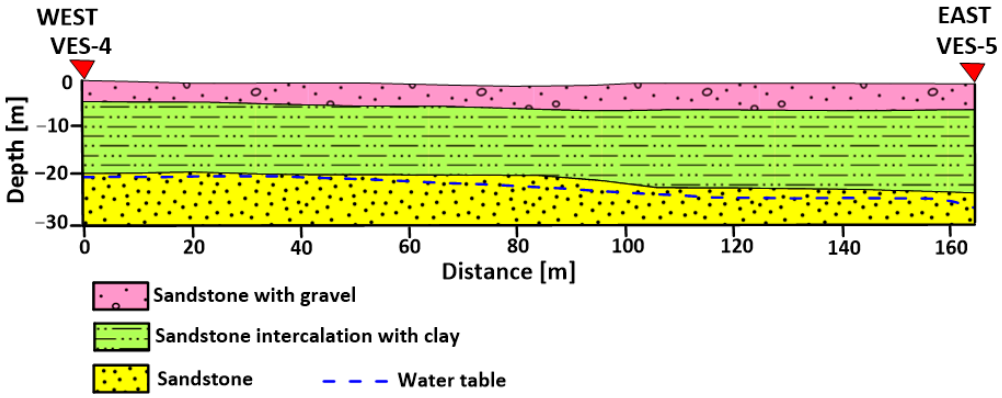

Figure 6. The southern geoelectric cross-section in the study area.

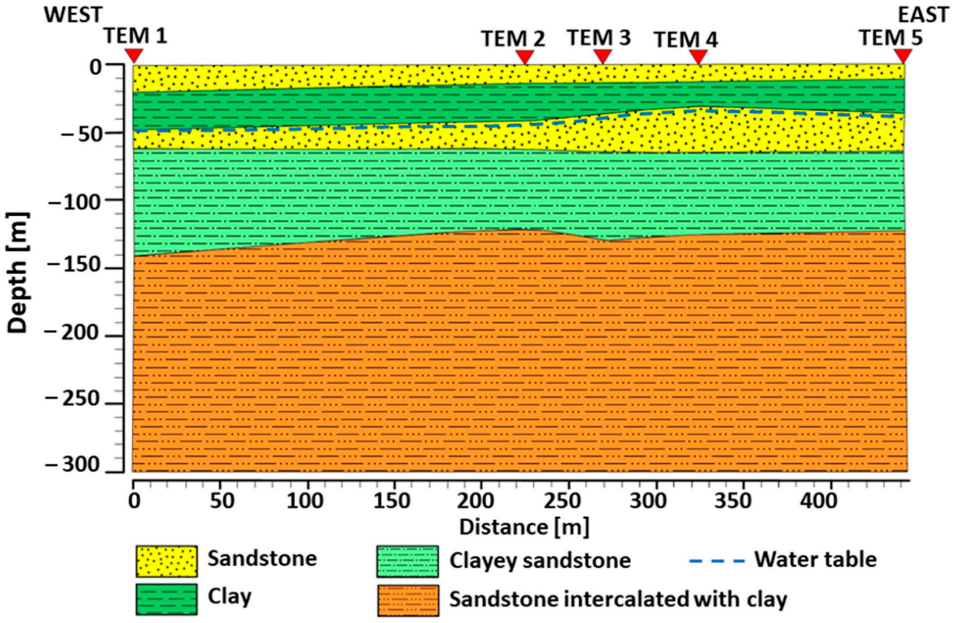

Figure 7. The northern electromagnetic cross-section in the study area.

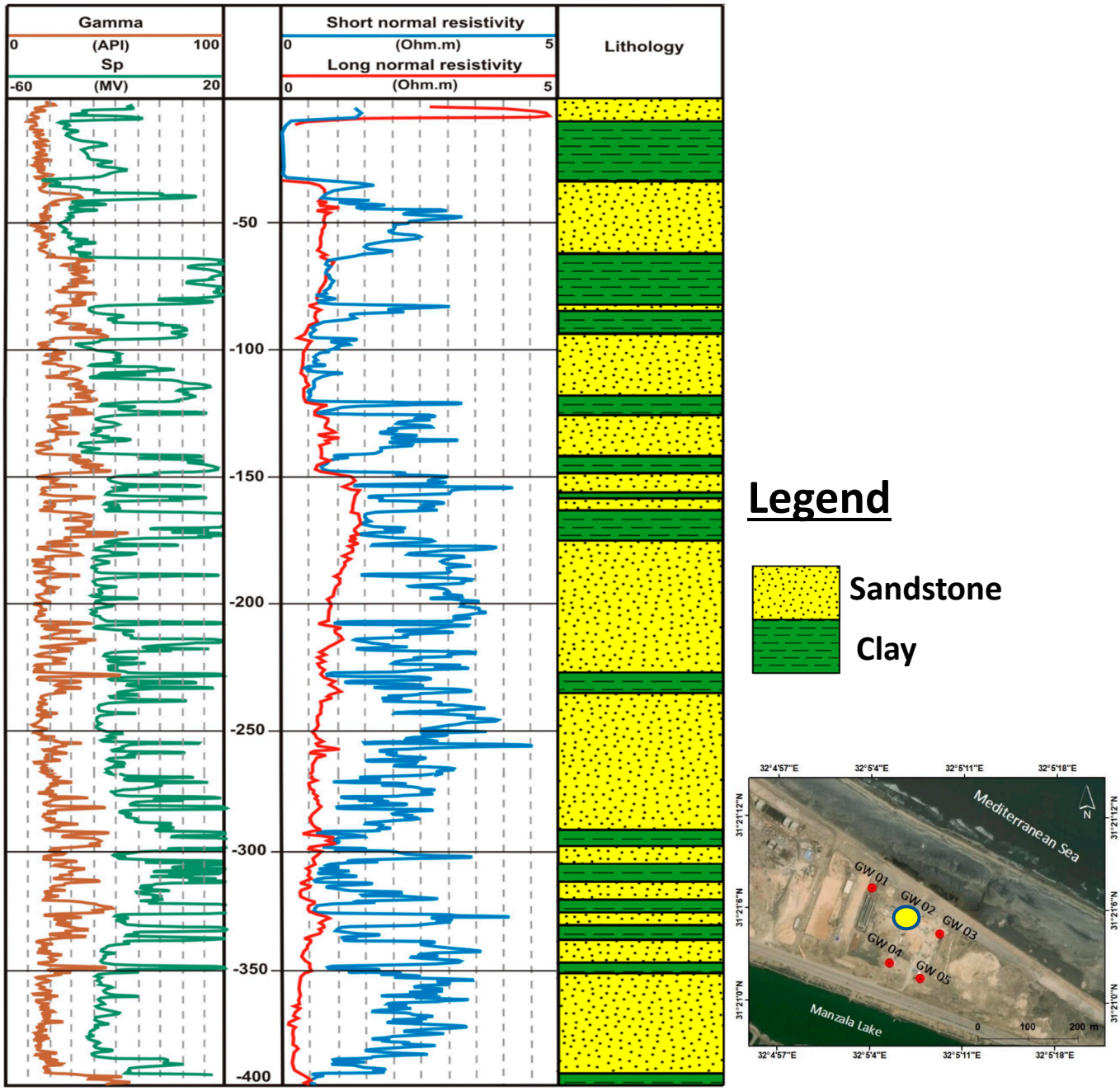

Figure 8. Gamma ray, SP, resistivity logs and the corresponding lithology in well GW02.

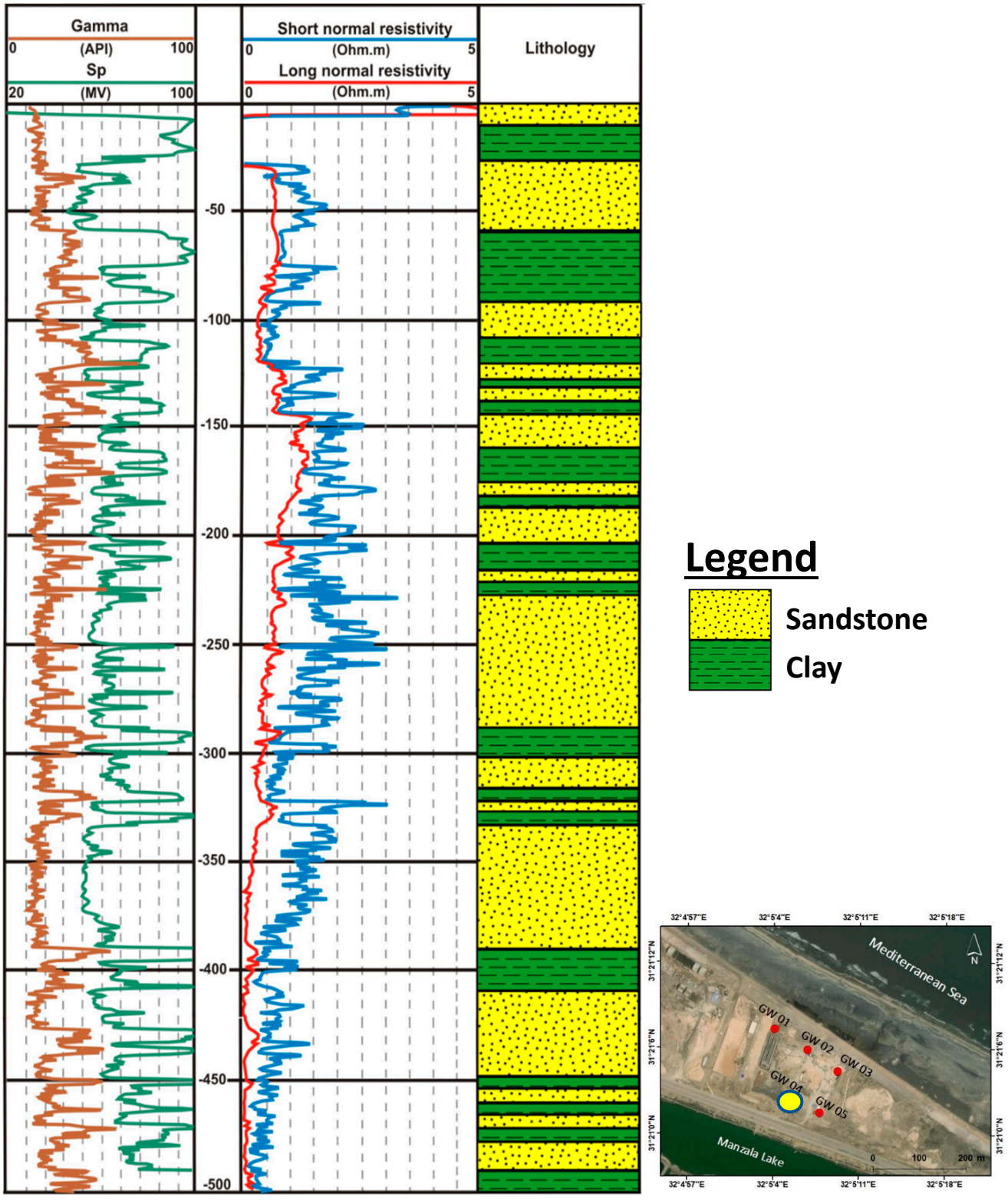

Figure 9. Gamma ray, SP, resistivity logs and the corresponding lithology in well GW04.

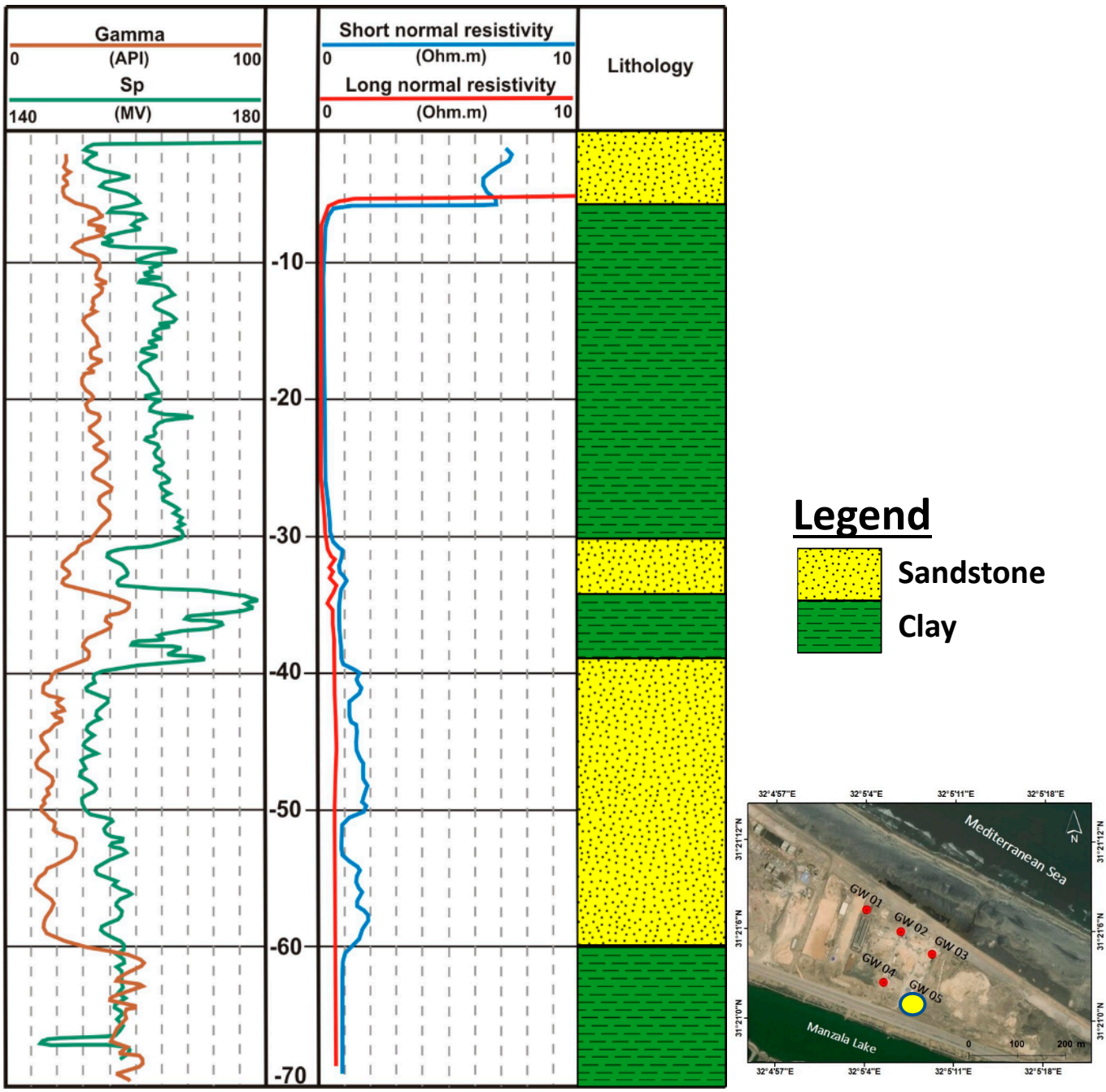

Figure 10. Gamma ray, SP, resistivity logs and the corresponding lithology in well GW05.

4.2. Aquifer Parameters

Three water-bearing layers (A, B, and C) with relative thicknesses of 90, 200, and 170 m, make up the groundwater aquifer system along the research region. The criteria of porosity, hydraulic conductivity, transmissivity, and storativity were established to assess the productivity of these aquifers.

The results of the sediment analyses that were conducted in the laboratory show that the average porosity values were 22%, 27.5%, and 25% for layers A, B, and C, respectively.

Five wells were used for the pumping test experiments, and Table 1 lists them all. These tests were carried out in each well by steady pumping for a specified period. The short-term relationship between the yield and the drawdown in the investigational borehole was initially established using step tests. The process of pumping the borehole consisted of

several steps, each with a variable discharge rate—typically, the rate increased with each step. Getting close to the estimated maximum yield of the borehole is the final step, and this step occurs when the pumping operation is continuous.

Table 1. Pumping test field data for three aquifers with in-situ chemical parameters and the estimated hydrogeological parameters.

	Continuous Pumping Tests				In Situ Chemical Parameters			Hydrogeological Parameters			
	Discharge Rate (m^3/h)	Drawdown (m)	Time (hour)	Layer	T (°C)	pH	EC (mS/cm)	Av. n (%)	Av. K (m/Day)	T (m^2/Day)	Av. S (m^2/Day)
GW01	250	13.38	24,48,72	Sandstone (A)	24.1–28.3	7.3–7.34	44.5–44.8	22	5.8–12.7	586–1270	2.1×10^{-3}
GW05	300	24.34	24		26.1–27.5	7.71–7.89	44.13–45.1				
GW02	300	31.33	24,72	Sandstone (B)	26.8–29.3	7.13–7.21	74.12–74.44	27.5	7.6–11.7	763–1170	1.8×10^{-3}
GW03	120	4.9	24,48,72		26.6–28.1	7.28–7.34	36.75–39.65				
GW04	300	16.87	24,72	Sandstone (C)	27.1–28.6	7.15–7.21	74.12–74.38	25	11.1–19.5	1110–1950	5.3×10^{-3}

Figures 11–13 show the observed drawdown data (blue squares) of the continuous pumping tests in the wells at different times (Table 1), and the black curves are the model solutions of the test analysis methods.

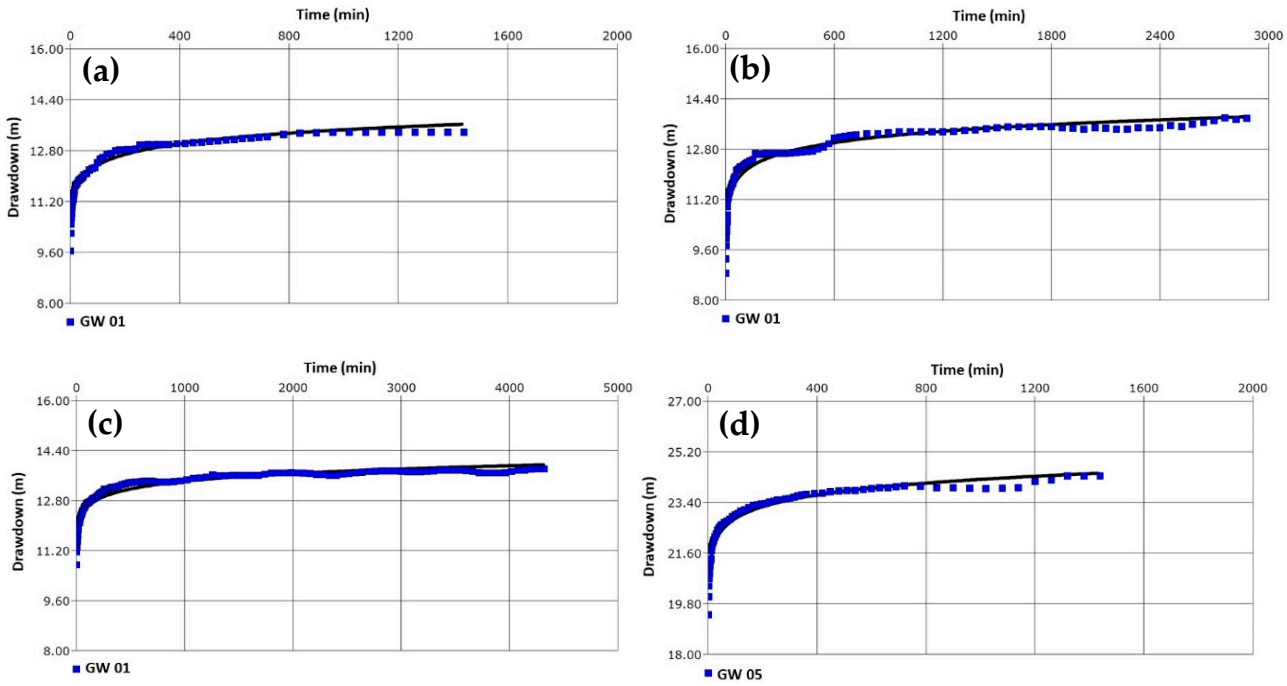

Figure 11. Continuous pumping test curves of unconfined aquifer (aquifer A): GW 01 for 24 h (**a**), 48 h (**b**), and 72 h (**c**), and GW 05 for 24 h (**d**).

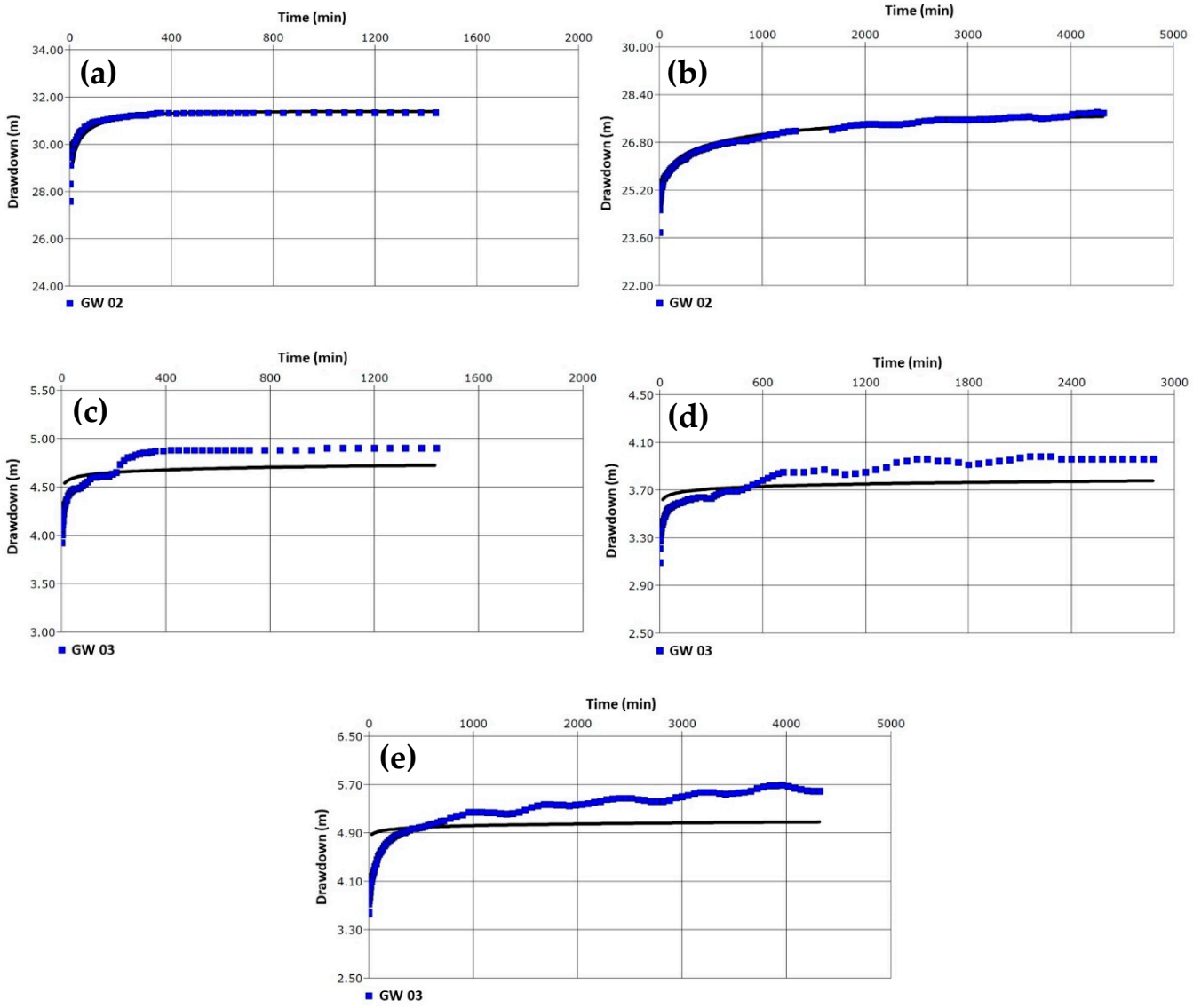

Figure 12. Continuous pumping test curves of leaky aquifer (aquifer B): GW 02 for 24 h (**a**) and 72 h (**b**), and GW 03 for 24 h (**c**), 48 h (**d**), and 72 h (**e**).

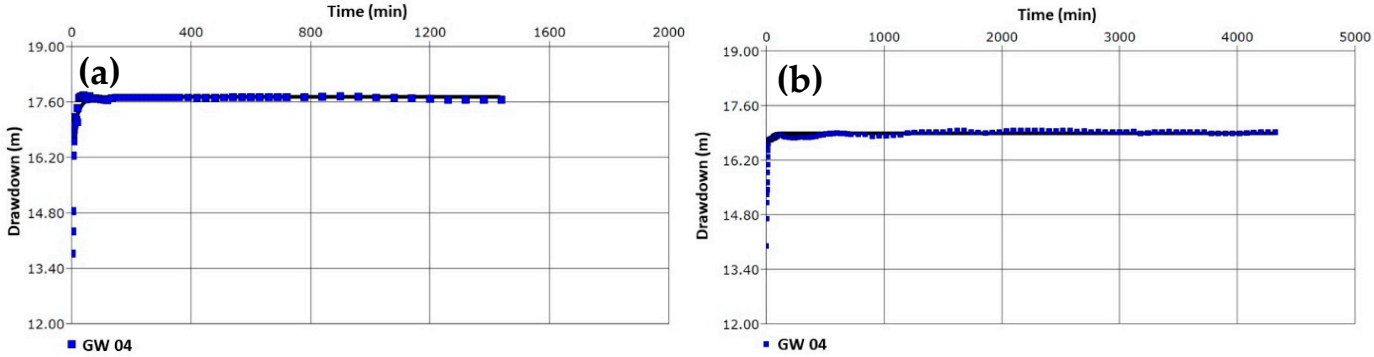

Figure 13. Continuous pumping test curves of deep confined aquifer (aquifer C): GW 04 for 24 h (**a**) and 72 h (**b**).

The results show high values of transmissivity, which ranged from 586 m^2/day to 1270 m^2/day in layer A, from 763 m^2/day to 1170 m^2/day in layer B, and from 1110 to 1950 m^2/day in layer C. As a result of the Mediterranean Sea's recharge, these aquifers

have high productivity [44]. The average values of storativity were 2.1×10^{-3}, 1.8×10^{-3}, and 5.3×10^{-3} m^2/day in layers A, B, and C, respectively.

4.3. Physicochemical Characteristics of Groundwater

Generally, the temperature, pH, and EC values were monitored, especially during the continuous pumping of wells, resulting in the following:

From wells GW01 and GW05, it is obvious that the shallow layer A had ranges of 24.1–28.3 °C, 7.3–7.7 pH, and 44.13–45.1 mS/cm.

From well GW 03, it is obvious that layer B had ranges of 26.6–28.1 °C, 7.28–7.34 pH, and 36.75–39.65 mS/cm.

From wells GW 02 and GW04, it is obvious that the deep layer C had ranges of 26.8–29.3 °C, 7.13–7.21 pH, and 74.12–74.44 mS/cm.

Table 2 shows the hydrogeochemical parameters of the groundwater samples that were analyzed to describe the chemical characteristics of the groundwater in the three layers and the permissible limits for drinking water purposes according to the World Health Organization (WHO, Geneva, Switzerland) standard [54].

Table 2. The physicochemical analyses of groundwater samples.

Physicochemical Parameters	Unit	Layer (A)				Layer (B)				WHO, 2011
		W1	W2	W3	Average	W4	W5	W6	Average	
pH	- - - - -	7.05	6.81	6.72	6.86	6.81	6.75	6.85	6.8	6.5–8.5
TDS	mg/L	32,410	32,270	32,410	32,363	26,950	27,580	27,510	27,346	1000
Major Cations										
Calcium (Ca^{2+})	mg/L	658	617	555	610	525	569	565	553	75
Magnesium (Mg^{2+})	mg/L	241	241	220	234	210	216	220	215	30
Sodium (Na^{+})	mg/L	9100	9250	9550	9300	7850	7950	7950	7916	200
Potassium (K^{+})	mg/L	300	290	210	266	170	175	180	175	10
Major Anions										
Carbonate (CO_3^{-})	mg/L	0	0	0	0	0	0	0	0	
Bicarbonate (HCO_3^{-})	mg/L	575	580	600	585	165	156	150	157	300
Sulfate (SO_4^{2-})	mg/L	1499	1495	1320	1438	1255	1300	1320	1291	250
Chloride (Cl^{-})	mg/L	14,005	14,214	14,720	14,313	12,100	12,200	12,250	12,183	250
Nitrite (NO_2^{-})	mg/L	<0.2	<0.2	<0.2		<0.2	<0.2	<0.2		
Nitrate (NO_3^{-})	mg/L	74	137	72	94	43	48	46	45	50
Fluoride (F^{-})	mg/L	1	0.92	<0.05	0.65	0.11	0.42	0.54	0.35	1.5
Heavy Metals										
Aluminum (Al)	mg/L	0.029	0.007	0.017	0.017	0.047	<0.007	0.04		0.1
Antimony (Sb)	mg/L	<0.009	<0.009	<0.009		<0.009	<0.009	<0.009		
Arsenic (As)	mg/L	<0.002	<0.002	<0.002		<0.026	<0.026	<0.026		0.01
Barium (Ba)	mg/L	0.038	0.039	0.036	0.037	0.078	0.092	0.109	0.093	0.7
Cadmium (Cd)	mg/L	0.003	<0.002	<0.002		<0.002	<0.002	<0.002		0.003
Chromium (Cr)	mg/L	<0.002	<0.002	<0.002		<0.002	<0.002	<0.002		
Cobalt (Co)	mg/L	<0.003	0.003	0.003		<0.003	<0.003	<0.003		
Copper (Cu)	mg/L	0.085	0.008	0.031	0.041	0.026	0.024	0.015	0.021	2
Iron (Fe)	mg/L	0.238	0.227	0.393	0.286	0.086	0.194	0.047	0.109	0.1
Lead (Pb)	mg/L	<0.007	<0.007	<0.007		<0.007	<0.007	<0.007		0.01
Manganese (Mn)	mg/L	1.163	1.188	1.19	1.18	1.545	1.599	1.663	1.6	0.05
Nickel (Ni)	mg/L	0.009	0.011	0.008	0.028	0.01	0.01	0.01	0.01	0.07
Selenium (Se)	mg/L	<0.007	<0.007	<0.007		<0.007	<0.007	<0.007		0.04

The groundwater was acidic to neutral in layers A and B, and there was no noticeable difference in terms of pH because the measured pH ranged from 6.75 to about 7 with an average of 6.8. These values are within the WHO guideline limits. The TDS values were slightly different and ranged from 32,270 mg/L to 32,410 mg/L with an average of about 32,360 mg/L in layer A, while ranging from 26,950 mg/L to 27,510 mg/L with an average of about 27,346 mg/L in layer B, indicating that the groundwater was saline in the study area (Figure 14) and exceeded the WHO limit.

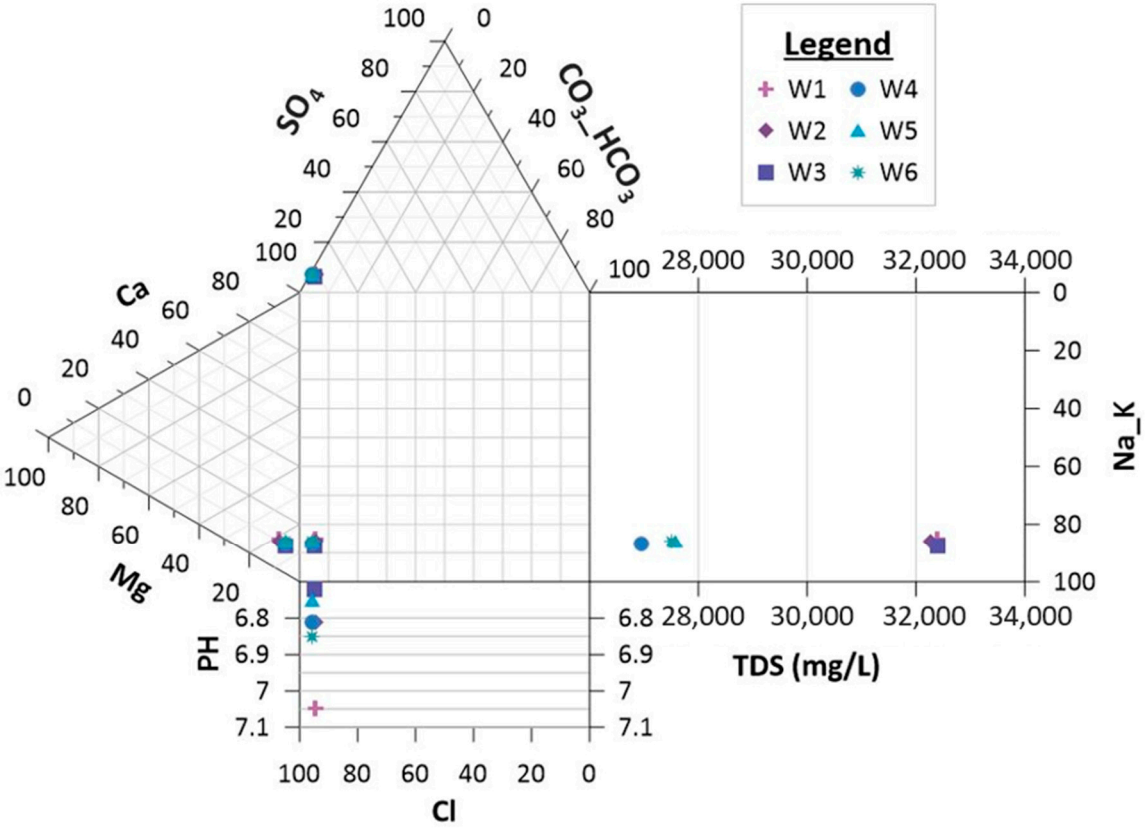

Figure 14. Durov plot for groundwater samples of unconfined and leaky aquifers.

Generally, the cation and anion concentration values of the groundwater in layer A were higher than in layer B. In layer A, the cation concentrations were in the order of $Na^+ > Ca^{2+} > K^+ > Mg^{2+}$ except for one sample, while in layer B, the cation concentrations were in the order of $Na^+ > Ca^{2+} > Mg^{2+} > K^+$ (Figure 14). The sodium concentration was the most dominant and ranged from 9100 mg/L to 9550 mg/L in layer A and from 7850 mg/L to 7950 mg/L in layer B. The calcium concentrations had the second-highest values and were in the ranges of 555–658 mg/L and 525–569 mg/L in layers A and B, respectively. The concentrations of magnesium and potassium had averages of 234 mg/L, and 266 mg/L in layer A and 215 mg/L and 175 mg/L in layer B. The cation concentration values (Ca^{2+}, Mg^{2+}, Na^+, and K^+) of the groundwater were higher than the WHO limits.

On the other hand, the anion concentration values of the groundwater in the two layers were in the order of $Cl^- > SO_4^{2-} > HCO_3^- > NO_3^-$. The chloride concentration was the most dominant, ranging from about 14,000 mg/L to 14,720 mg/L with an average of 14,313 mg/L in layer A, and ranging from 12,100 mg/L to 12,250 mg/L with an average of 12,183 mg/L in layer B. The concentrations of SO_4^{2-} ranged within 1320–1500 mg/L and 1255–1320 mg/L in layers A and B, respectively. The concentrations of HCO_3^- and NO_3^- had averages of 585 mg/L and 94 mg/L in layer A and 157 mg/L and about 45 mg/L in layer B. These anion concentrations of groundwater in the two layers were above the concentration limits of WHO, except for the nitrate concentration in layer B. All

groundwater samples in layers A and B were of Na-Cl type due to the closeness of the Mediterranean Sea and seawater intrusion in the study area.

Fluoride (F^-) is an essential element for human health [55–57]. Layers A and B had averages of 0.65 mg/L and 0.35 mg/L respectively. The heavy metal concentrations were below the WHO limit, which means there is no health risk except for the Mn concentration, which can be lowered by the desalination process.

5. Conclusions

Recently, the government has become interested in looking for fresh water resources. Saline groundwater desalination is one of these resources, particularly in coastal regions. The study area serves as an example of how desalination plants rely on groundwater as a source of water based on an accurate and comprehensive methodology. Therefore, geophysical techniques, pumping tests, water sampling, and groundwater quality were performed. The findings indicate that there are three water-bearing layers named, A, B, and C. After hydrogeological analyses to ascertain their characteristics, such as porosity, hydraulic conductivity, storativity, and transmissivity, it became evident that layer A is the best of them.

The groundwater within layers A and B were chemically evaluated. Geochemical analysis indicated a decrease in the groundwater salinity with depth. The shallow layer A had a greater TDS and higher concentrations of major ions and heavy metals compared to layer B; however, both layers were dominated by the Na-Cl type.

This study shows that the deep layer B had higher productivity, lower salinity, and lower element concentrations compared to the shallow layer A. Thus, we recommend the use of layer B, which has higher quality characteristics and can be improved by desalination, for domestic and industrial uses.

This integration of multiple approaches for coastal aquifer characterization and saline groundwater desalination could provide decision-makers with a clear picture of the aquifer and help with its future development. Our findings of using this aquifer as an alternative to oil-polluted seawater can be crucially efficient for future applications not only in Egypt but also in other coastal areas where groundwater is regularly salinized. The study could be a step forward for a better understanding of the coastal aquifer characteristics as well as water resource utilization and management, especially in highly water-scarce regions, such as Egypt and other arid regions.

Author Contributions: Conceptualization, M.A. and H.A.-A.A.-B.; methodology, M.A., A.G. and T.M.H.; validation, M.A. and H.A.-A.A.-B.; writing—original draft preparation, M.A. and H.A.-A.A.-B.; supervision, writing—review and editing, A.G., M.H.G., T.M.H., M.S. and F.M.M. All authors have read and agreed to the published version of the manuscript.

Funding: This research study received no external funding.

Institutional Review Board Statement: Not applicable.

Informed Consent Statement: Not applicable.

Data Availability Statement: Not applicable.

Conflicts of Interest: The authors declare no conflict of interest.

References

1. Gleick, P.H. Global Freshwater Resources: Soft-Path Solutions for the 21st Century. *Science* **2003**, *302*, 1524–1528. [CrossRef] [PubMed]
2. Hoekstra, A.Y.; Mekonnen, M.M. The Water Footprint of Humanity. *Proc. Natl. Acad. Sci USA* **2012**, *109*, 3232–3237. [CrossRef] [PubMed]
3. Aboel Ghar, M.; Shalaby, A.; Tateishi, R. Agricultural Land Monitoring in the Egyptian Nile Delta Using Landsat Data. *Int. J. Environ. Stud.* **2004**, *61*, 651–657. [CrossRef]
4. El-Sadek, A. Water Desalination: An Imperative Measure for Water Security in Egypt. *Desalination* **2010**, *250*, 876–884. [CrossRef]

5. Ghaffour, N.; Missimer, T.M.; Amy, G.L. Technical Review and Evaluation of the Economics of Water Desalination: Current and Future Challenges for Better Water Supply Sustainability. *Desalination* **2013**, *309*, 197–207. [CrossRef]
6. Bhojwani, S.; Topolski, K.; Mukherjee, R.; Sengupta, D.; El-Halwagi, M.M. Technology Review and Data Analysis for Cost Assessment of Water Treatment Systems. *Sci. Total Environ.* **2019**, *651*, 2749–2761. [CrossRef]
7. Park, K.; Kim, J.; Yang, D.R.; Hong, S. Towards a Low-Energy Seawater Reverse Osmosis Desalination Plant: A Review and Theoretical Analysis for Future Directions. *J. Memb. Sci.* **2020**, *595*, 117607. [CrossRef]
8. Boumaiza, L.; Chesnaux, R.; Drias, T.; Walter, J.; Huneau, F.; Garel, E.; Knoeller, K.; Stumpp, C. Identifying Groundwater Degradation Sources in a Mediterranean Coastal Area Experiencing Significant Multi-Origin Stresses. *Sci. Total Environ.* **2020**, *746*, 141203. [CrossRef]
9. El-Magd, I.A.; Zakzouk, M.; Ali, E.M.; Abdulaziz, A.M. An Open Source Approach for Near-Real Time Mapping of Oil Spills along the Mediterranean Coast of Egypt. *Remote Sens.* **2021**, *13*, 2733. [CrossRef]
10. Sherif, M.M.; Singh, V.P. Effect of Climate Change on Sea Water Intrusion in Coastal Aquifers. *Hydrol. Process.* **1999**, *13*, 1277–1287. [CrossRef]
11. Bear, J.; Cheng, A.H.-D.; Sorek, S.; Ouazar, D.; Herrera, I. *Seawater Intrusion in Coastal Aquifers: Concepts, Methods and Practices*; Springer Science & Business Media: Berlin, Germany, 1999; Volume 14, ISBN 0792355733.
12. Pennington, B.T.; Sturt, F.; Wilson, P.; Rowland, J.; Brown, A.G. The Fluvial Evolution of the Holocene Nile Delta. *Quat. Sci. Rev.* **2017**, *170*, 212–231. [CrossRef]
13. Dahab, K.A. Hydrogeological Evolution of the Nile Delta after the High Dam Construction. Ph.D. Dissertation, Geology Department, Faculty of Science, Menoufia University, Menoufia, Egypt, 1993.
14. Farid, M.S. Management of Groundwater System in the Nile Delta. Ph.D. Thesis, Cairo University, Giza, Egypt, 1985.
15. Stanley, D.J. Subsidence in the Northeastern Nile Delta: Rapid Rates, Possible Causes, and Consequences. *Science* **1988**, *240*, 497–500. [CrossRef]
16. Stanley, J.-D.; Clemente, P.L. Increased Land Subsidence and Sea-Level Rise Are Submerging Egypt's Nile Delta Coastal Margin. *GSA Today* **2017**, *27*, 4–11. [CrossRef]
17. Geriesh, M.H.; Balke, K.-D.; El-Rayes, A.E.; Mansour, B.M. Implications of Climate Change on the Groundwater Flow Regime and Geochemistry of the Nile Delta, Egypt. *J. Coast. Conserv.* **2015**, *19*, 589–608. [CrossRef]
18. Abdel-Moati, M.A.R.; El-Sammak, A.A. Man-Made Impact on the Geochemistry of the Nile Delta Lakes. A Study of Metals Concentrations in Sediments. *Water. Air. Soil Pollut.* **1997**, *97*, 413–429. [CrossRef]
19. Abd-Elhamid, H.; Javadi, A.; Abdelaty, I.; Sherif, M. Simulation of Seawater Intrusion in the Nile Delta Aquifer under the Conditions of Climate Change. *Hydrol. Res.* **2016**, *47*, 1198–1210. [CrossRef]
20. Mabrouk, M.; Jonoski, A.; Oude Essink, G.H.P.; Uhlenbrook, S. Assessing the Fresh–Saline Groundwater Distribution in the Nile Delta Aquifer Using a 3D Variable-Density Groundwater Flow Model. *Water* **2019**, *11*, 1946. [CrossRef]
21. Martínez, D.; Bocanegra, E. Hydrogeochemistry and Cation-Exchange Processes in the Coastal Aquifer of Mar Del Plata, Argentina. *Hydrogeol. J.* **2002**, *10*, 393–408. [CrossRef]
22. Andersen, M.S.; Nyvang, V.; Jakobsen, R.; Postma, D. Geochemical Processes and Solute Transport at the Seawater/Freshwater Interface of a Sandy Aquifer. *Geochim. Cosmochim. Acta* **2005**, *69*, 3979–3994. [CrossRef]
23. Ataie-Ashtiani, B.; Volker, R.E.; Lockington, D.A. Tidal Effects on Sea Water Intrusion in Unconfined Aquifers. *J. Hydrol.* **1999**, *216*, 17–31. [CrossRef]
24. Zhang, Q.; Wang, Z. Spatial Prediction of Loose Aquifer Water Abundance Mapping Based on a Hybrid Statistical Learning Approach. *Earth Sci. Inform.* **2021**, *14*, 1349–1365. [CrossRef]
25. Riolo, A. Maltese Experience in the Application of Desalination Technology. *Desalination* **2001**, *136*, 115–124. [CrossRef]
26. Missimer, T.M.; Ghaffour, N.; Dehwah, A.H.A.; Rachman, R.; Maliva, R.G.; Amy, G. Subsurface Intakes for Seawater Reverse Osmosis Facilities: Capacity Limitation, Water Quality Improvement, and Economics. *Desalination* **2013**, *322*, 37–51. [CrossRef]
27. Sola, F.; Vallejos, A.; López-Geta, J.A.; Pulido-Bosch, A. The Role of Aquifer Media in Improving the Quality of Seawater Feed to Desalination Plants. *Water Resour. Manag.* **2013**, *27*, 1377–1392. [CrossRef]
28. Park, N.; Kim, S.; Shi, L.; Song, S. Field Validation of Simulation-Optimization Model for Protecting Excessive Pumping Wells. In Proceedings of the 20th Salt Water Intrusion Meeting, Naples, FL, USA, 23–27 June 2008.
29. Park, N.; Lei, C.; Chanjong, L. Analytical Method for Preliminary Management of Pumping and Injection in Coastal Areas. In Proceedings of the 20th Salt Water Intrusion Meeting, Naples, FL, USA, 23–27 June 2008.
30. Thammanu, S.; Marod, D.; Han, H.; Bhusal, N.; Asanok, L.; Ketdee, P.; Gaewsingha, N.; Lee, S.; Chung, J. The Influence of Environmental Factors on Species Composition and Distribution in a Community Forest in Northern Thailand. *J. For. Res.* **2021**, *32*, 649–662. [CrossRef]
31. Wu, Q.; Jiang, X.; Lu, Q.; Li, J.; Chen, J. Changes in Soil Organic Carbon and Aggregate Stability Following a Chronosequence of Liriodendron Chinense Plantations. *J. For. Res.* **2021**, *32*, 355–362. [CrossRef]
32. Liao, C.; Tian, Q.; Liu, F. Nitrogen Availability Regulates Deep Soil Priming Effect by Changing Microbial Metabolic Efficiency in a Subtropical Forest. *J. For. Res.* **2021**, *32*, 713–723. [CrossRef]
33. Shahabi, M.P.; McHugh, A.; Ho, G. Environmental and Economic Assessment of Beach Well Intake versus Open Intake for Seawater Reverse Osmosis Desalination. *Desalination* **2015**, *357*, 259–266. [CrossRef]

34. Pulido-Bosch, A.; Vallejos, A.; Sola, F. Methods to Supply Seawater to Desalination Plants along the Spanish Mediterranean Coast and Their Associated Issues. *Environ. Earth Sci.* **2019**, *78*, 322. [CrossRef]
35. Dehwah, A.H.A.; Al-Mashharawi, S.; Kammourie, N.; Missimer, T.M. Impact of Well Intake Systems on Bacterial, Algae, and Organic Carbon Reduction in SWRO Desalination Systems, SAWACO, Jeddah, Saudi Arabia. *Desalin. Water Treat.* **2015**, *55*, 2594–2600. [CrossRef]
36. Abdel-Jawad, M.; Ebrahim, S. Beachwell Seawater Intake as Feed for an RO Desalting System. *Desalination* **1994**, *99*, 57–71. [CrossRef]
37. Rachman, R.M.; Li, S.; Missimer, T.M. SWRO Feed Water Quality Improvement Using Subsurface Intakes in Oman, Spain, Turks and Caicos Islands, and Saudi Arabia. *Desalination* **2014**, *351*, 88–100. [CrossRef]
38. EEAA. *Egypt Second National Communication under the United Nations Framework Convention on Climate Change (UNFCCC)*; EEAA: Cairo, Egypt, 2010.
39. Negm, A.M.; Sakr, S.; Abd-Elaty, I.; Abd-Elhamid, H.F. An Overview of Groundwater Resources in Nile Delta Aquifer. In *Groundwater in the Nile Delta*; Springer: Berlin/Heidelberg, Germany, 2018; pp. 3–44.
40. Website. Available online: https://www.worldweatheronline.com/port-said-weather-averages/bur-said/eg.aspx (accessed on 18 May 2021).
41. Zaghloul, Z.M.; Taha, A.A.; Hegab, O.; El Fawal, F. The Neogene-Quaternary Sedimentary Basins of the Nile Delta. *Egypt. J. Geol.* **1977**, *21*, 1–19.
42. El-Fayoumy, I.F. Geology of Groundwater Supplies in the Eastern Region of the Nile Delta and Its Extension in North Sinai. Ph.D. Thesis, Faculty of Science, Cairo University, Cairo, Egypt, 1968.
43. Abdelfattah, M.; Abu-Bakr, H.A.-A.; Gaber, A.; Geriesh, M.H.; Elnaggar, A.Y.; El Nahhas, N.; Hassan, T.M. Proposing the Optimum Withdrawing Scenarios to Provide the Western Coastal Area of Port Said, Egypt, with Sufficient Groundwater with Less Salinity. *Water* **2021**, *13*, 3359. [CrossRef]
44. Sestini, G. Nile Delta: A Review of Depositional Environments and Geological History. *Geol. Soc. Lond. Spec. Publ.* **1989**, *41*, 99–127. [CrossRef]
45. RIGW. Hydrogeological Map of Nile Delta, Scale 1: 500,000, 1st ed.; (Nile Delta). 1992.
46. Rider, M. *The Geological Interpretation of Well Logs Second Edition*; Rider–French Consult. Ltd.: Sutherland, UK, 2000; pp. 126–128.
47. Telford, W.M.; Telford, W.M.; Geldart, L.P.; Sheriff, R.E. *Applied Geophysics*; Cambridge University Press: Cambridge, UK, 1990; ISBN 0521339383.
48. Fiser-Nagy, Á.; Varga-Tóth, I.; Tóth, T.M. Lithology Identification Using Open-Hole Well-Log Data in the Metamorphic Kiskunhalas-NE Hydrocarbon Reservoir, South Hungary. *Acta Geod. Geophys.* **2014**, *49*, 57–78. [CrossRef]
49. Das, B.; Chatterjee, R. Well Log Data Analysis for Lithology and Fluid Identification in Krishna-Godavari Basin, India. *Arab. J. Geosci.* **2018**, *11*, 231. [CrossRef]
50. Ellis, D.V.; Singer, J.M. *Well Logging for Earth Scientists*; Springer: Berlin/Heidelberg, Germany, 2007; Volume 692.
51. El-Khodre, A.S.; Bedaiwy, M.N.A. Experimental Characterization of Physio-Chemical, Hydrodynamic and Mechanical Properties of Two Typical Egyptian Soils. *Tishreen Univ. J. Res. Sci. Stud. Sci. Ser.* **2008**, *30*, 169–191.
52. APHA. *Standard Methods for the Examination of Water and Wastewater*; American Public Health Association, American Water Works Association, Water Environment Federation: Washington, DC, USA, 2005.
53. Durov, S.A. Natural Waters and Graphical Representation of Their Composition: Doklady Akademii Nauk. *Union Sov. Social. Repub.* **1948**, *59*, 87–90.
54. WHO. *Guidelines for Drinking-Water Quality*; WHO: Geneva, Switzerland, 2011; Volume 216, pp. 303–304.
55. Currell, M.; Cartwright, I.; Raveggi, M.; Han, D. Controls on Elevated Fluoride and Arsenic Concentrations in Groundwater from the Yuncheng Basin, China. *Appl. Geochem.* **2011**, *26*, 540–552. [CrossRef]
56. Li, P.; Qian, H.; Wu, J.; Chen, J.; Zhang, Y.; Zhang, H. Occurrence and Hydrogeochemistry of Fluoride in Alluvial Aquifer of Weihe River, China. *Environ. Earth Sci.* **2014**, *71*, 3133–3145. [CrossRef]
57. Wu, J.; Li, P.; Qian, H. Hydrochemical Characterization of Drinking Groundwater with Special Reference to Fluoride in an Arid Area of China and the Control of Aquifer Leakage on Its Concentrations. *Environ. Earth Sci.* **2015**, *73*, 8575–8588. [CrossRef]